

Supra-Binary Polarization in a Ferroelectric Nanowire

Wentao Xu, Lihua Wang, David ChangMo Yang, Amir Hajibabaei, Yeongjun Lee, Cheolmin Park, Tae-Woo Lee,* and Kwang S. Kim*

The prediction and observation of supra-binary polarization in a ferroelectric nanowire (FNW) covered with a semicylindrical gate that provides an anisotropic electric field in the FNW are reported. There are gate-voltage-driven transitions between four polarization states in the FNW's cross-section, dubbed vertical-up, vertical-down, radial-in, and radial-out. They are determined by the interplay between the spatial depolarization energy and the free energy induced by an anisotropic external electric field, in clear distinction from the conventional film-based binary ferroelectricity. When the FNW is mounted on a biased graphene nanoribbon (GNR), these transitions induce exotic current–voltage hysteresis in the FNW–GNR transistor. This discovery suggests new operating mechanisms of ferroelectric devices. In particular, it enables intrinsic quaternary-digit information manipulation in parallel to the bit manipulation employed in conventional data storage.

can undergo an abrupt jump which is a typical hallmark of first-order transition between different phases or states and the reported transitions have been mostly binary.^[5] Memory devices built from these materials are being proposed as new approaches to nonvolatile random-access memory, in which arrays of ferroelectric cells store binary information that can be altered in response to an external electric field. Any improvement of the storage capacity thereupon would involve increasing the number of units. Given the quantum limit which foretells the impending curtailment of such growth, exploring the possibility of storing multiple bits per unit is considered as an alternative. Recent nonmaterial innovations

1. Introduction

A ferroelectric material exhibits persistent polarization when exposed to a weak external electric field.^[1–4] The polarization

have demonstrated multibit data storage units with the conventional binary ferroelectricity, by combining translational ferroelectric domain strips^[6] or many ferroelectric nanoparticles.^[7] Recently, ternary metal oxide semiconductor technology based on tunneling appeared.^[8] These approaches improve the ratio of read-and-write heads to storage units.

Exploration of ferroelectric properties of organic polymers has been made by evoking microscopic processes such as charge transfer.^[9] Ferroelectric superdomain dynamics in ferroelectric–ferroelastic films along with switching has been reviewed.^[10] Meanwhile, the phenomenological and macroscopic Landau–Ginzburg theory (LGT)^[5] continues to be used for general ferroelectric materials.^[11] For instance, the Landau double-well energy landscape in a binary ferroelectric layer was recently revealed.^[12] In LGT, the free energy F is built upon a dipole density field $\vec{P}(\vec{r})$ describing the polarization in a ferroelectric material. The system must settle into one of the minima of F , thus yielding a specific polarization and breaking the symmetry spontaneously. The minima and the energy barrier between them evolve with the external electric field \vec{E}_{ext} . A transition of polarization states happens when the system overcomes the energy barrier to choose another minimum of F . Of interest in this work are supra-binary ferroelectric properties in a ferroelectric nanowire (FNW), for which LGT is extended.

2. Results and Discussion

Here, we show that the free energy terms due to radial and vertical depolarizations in a FNW compete with each other depending on $\vec{P}(\vec{r})$ and domains. This competition, along with the interaction between \vec{P} and \vec{E}_{ext} , may induce new transitions between four polarization configurations in the FNW's


Prof. W. Xu, Dr. Y. Lee, Prof. T.-W. Lee
 Department of Materials Science and Engineering
 Institute of Engineering Research
 Research Institute of Advanced Materials
 Seoul National University
 1 Gwanak-ro, Gwanak-gu, Seoul 08826, Republic of Korea
 E-mail: twlees@snu.ac.kr

Prof. W. Xu
 Institute of Optoelectronic Thin Film Devices and Technology
 Key Laboratory of Optoelectronic Thin Film Device and Technology of Tianjin
 Nankai University
 Tianjin 300350, P. R. China

Dr. L. Wang, Dr. D. C. Yang, Dr. A. Hajibabaei, Prof. K. S. Kim
 Department of Chemistry
 School of Natural Science
 Center for Superfunctional Materials
 Ulsan National Institute of Science and Technology (UNIST)
 50 UNIST-gil, Ulsan 44919, Republic of Korea
 E-mail: kimks@unist.ac.kr

Prof. C. Park
 Department of Materials Science and Engineering
 Yonsei University
 50 Yonsei-ro, Seoul 03722, Republic of Korea

Prof. K. S. Kim
 Department of Physics
 Ulsan National Institute of Science and Technology (UNIST)
 50 UNIST-gil, Ulsan 44919, Republic of Korea

 The ORCID identification number(s) for the author(s) of this article can be found under <https://doi.org/10.1002/adma.202101981>.

DOI: 10.1002/adma.202101981

cross-section, dubbed vertical-up, vertical-down, radial-in, and radial-out, that provide candidates for a multiary digit per unit.

To test this possibility, we deposited a straight array electrospun FNWs on a large area with individual control over positioning and alignment, perpendicular to an underlying graphene nanoribbon (GNR). Next, semicylindrical metallic electrodes on top of the FNW and two contact pads under the FNW's rims were self-aligned. A field-effect transistor (FET) was then built, combining a top-gated FNW and a pre-etched biased GNR underneath it. We chose the poly(vinylidene fluoride-trifluoroethylene) organic copolymer P(VDF_{0.7}-TrFE_{0.3}) as the printed material.^[3] Its nonlinear nature and easy processability provide great potential for ferroelectricity.^[13,14]

The devices were fabricated using all-nanowire (NW)-templated lithography and self-alignment approaches (Figure 1). To avoid additional contaminants that complicate electrical characteristics, the process did not use traditional lithography. A graphene sheet was synthesized by chemical vapor deposition on Cu foil,^[15] and then transferred to a highly doped silicon wafer coated with a 300 nm SiO₂ layer.^[16] An array of parallel poly(vinyl carbazole) (PVK) NWs with a pitch of 50 μm was printed on the graphene sheet to provide protective masks.^[17,18] Electrohydrodynamic NW printing produces NWs with nearly perfect circular cross-section.^[16] O₂ plasma was used to etch away the unprotected regions to leave GNRs beneath the narrow contact between cylindrical NWs and graphene. PVK masks were removed by brief sonication in chloroform to leave GNRs with individual width of ≈ 30 nm. A second series of PVK

NWs was then printed in parallel but with staggered GNRs, which later served as separators of the metal pads. Constant-pitched P(VDF-TrFE) FNWs with diameter ≈ 250 nm in β -phase (Figures S1–S4, Supporting Information) were printed on the same plane but vertically to the longitudinal directions of GNRs. A thin metal layer (3 nm Ti/35 nm Au) was then deposited by thermal evaporation, and the layer was directly separated into several regions (Figures S5,S6), in which four pads are in direct contact with the substrate, with two metallic lines on PVK NWs, and with one metallic line on P(VDF-TrFE) FNW. Thus, the FNW is covered with a semicircular cross-sectioned electrode. Consequently, the source, drain, and gate electrodes were formed in one step. Two of the pads in contact with two ends of GNRs functioned as source and drain electrodes.

Most existing studies used P(VDF-TrFE) as thin films. Attempts to explore its ferroelectric switching mechanisms and electronic applications in NWs are rare, due to the lack of both theoretical foundations and appropriate fabrication techniques. Since the macromolecular direction of P(VDF-TrFE) chains lies along the FNW itself, the polarization in the longitudinal direction is averaged out to zero despite the presence of skew linkages.^[19–21] Thus, we will assume translational symmetry and confine our discussion to FNW's cross-section. A recent molecular dynamics simulation of the stretched P(VDF-TrFE) nanofiber with diameters of a few nanometers suggested that multiple ferroelectric domains will form in the cross-section when the diameter increases.^[22] Inside a cross-section, the alignment of those domains after relaxation tends to yield an overall rotary vertex which stems from the circular surface boundary. For comparison, the domain size in polymer films is no more than 40 nm with the domain wall width of ≈ 7 nm.^[23]

As the diameter increases, more domains asymptotically tend to form and align more randomly (even before reaching the size of 250 nm used in our case), and the line integral of the boundary restriction becomes dominated by the volume integral of other free energy terms, which results in blurred domain boundaries.^[24] This implies that our material hosts an effective multidomain ferroelectricity.^[25] In the present study, we have deployed electrospinning to stretch and then print P(VDF-TrFE) NWs (Methods S1–S6, Supporting Information). We observed exotic current–voltage (I – V) responses on GNR, which are attributed to novel transitions among four states by both radial and vertical alignments of the dipole density field in the FNW (Videos S1 and S2, Supporting Information). In what follows, we propose a theoretical model that explains well the observed phenomenon.

The metallic gate line provides the FNW with an anisotropic electric field (Methods S7 and S8, Supporting Information) which is approximately radial toward the upper half circle (part 1) and approximately vertical in the lower half circle (part 2), as shown in Figure 1c. These two topologies of the electric field each induce corresponding spontaneous polarizations that can be in two opposite directions. Numerical results predict spontaneous radial polarization in the FNW^[26] with $\vec{P} = 0$ at $\vec{r} = 0$ (center) and then show that the polarization will switch between radial-in and radial-out in the FNW when the radial external field \vec{E}_{ext} varies.^[27,28] The radial polarization was confirmed in experiment^[29] using an electron beam to create a radial external field. We recall that the vertical and lateral of piezoresponse

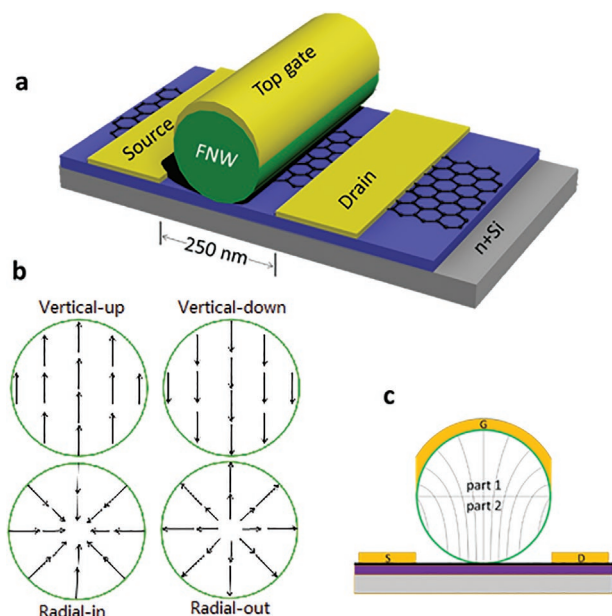


Figure 1. a) Schematic of the one-step self-aligned GNR FET using FNWs with semicircular top-gate. Preadigned GNRs were patterned from chemical vapor deposition-grown graphene by using organic NW lithography. P(VDF-TrFE) FNW is used as the ferroelectric gate insulator on which a continuous gate was formed. PVK NW is used as a separator. A 40 nm Au layer was self-aligned in one step during evaporation into source (S), drain (D), and gate (G) electrodes. b) Four polarization configurations in FNW's cross-section (vertical-in/out and radial-in/out). c) External electrical field configuration in the cross-section of the FNW, simulated by the finite element method.

force microscopy signals in P(VDF-TrFE) collagen revealed polar anisotropy of the electromechanical properties along the axes of the fibrils.^[30] We point out that the vertical and radial polarizations may compete when two orientations of the electric field coexist and supra-binary transition/switching may occur among vertical-up-down and radial-in-out states when the external field sweeps within certain ranges. The depolarization field \vec{E}_D in the FNW is induced by two sources. The first source is the charge on the inner surface resulting from the dipole-surface projection $\hat{S} \cdot \vec{P}(r=R)$ where \hat{S} is the unit normal vector at a surface point $r=R$ (Method S8, Supporting Information). The radial polarization in a circular cross-section is the uncommon case in which this term is switched off without any surface charge compensation. Another such case is with a rotational dipole field, but does not apply to our system as there is no rotational external field applied. The second source is the divergence of \vec{P} , $(\vec{\nabla} \cdot \vec{P})$. It vanishes for a vertical polarization configuration but exists as $-\rho_b(\vec{r})/\epsilon_{\text{FNW}}$ for a radial polarization configuration. Putting these two sources together, the depolarization field has very distinct forms depending on the topology of polarization (Table S1, Supporting Information). The free energy penalty due to depolarization in a radial polarization configuration is much weaker compared with that in a vertical configuration (Method S8, Supporting Information). While \vec{E}_D is more rigidly controlled by the magnitude P_0 of spontaneous polarization, \vec{E}_{ext} is sensitive to the gate voltage V_G . Therefore, the two fields give competing contributions to the free energy. As a result, the FNW shows four states of polarization in the cross-section of the FNW during sweeps of V_G : radial-in, radial-out, vertical-up, and vertical-down. Depending on the sweeping range and manner, it undergoes type I: no state transition (−2 to 2 V, Figure 2a); type II: transition between two states (−5 to 6 V, Figure 2b); type III: transition among all states (−6 to 6 V, Figure 2c). Different transitions are found as a function of the applied voltage: i) type I: $|V_G| < 3.5$ V, ii) type II: $4.5 \text{ V} < |V_G| < 5.5$ V, and iii) type III: $6 \text{ V} < |V_G|$ (i.e., the transition voltages for types I and II: $|V_G| \approx 4$ V and the transition voltages for types II and III: $|V_G| \approx 5.5$ –6.0 V). The resistance on/off switching ratio between different polar states is $\approx 40\%$ (Figure 2c, from V8 to V1 state at $V_G \approx 5.5$ V), more than $\approx 10\%$ which is feasible for reading/writing, but smaller than the largest on/off ratios of the binary states (100–1000%).^[31,32] The value of 40% for the quaternary states is still impressive, since the value is much more than $\approx 10\%$ which is feasible for reading/writing. The relatively smaller ratio is attributed to the irregular electric field distribution in the transverse direction of the GNR (see simulated Figure S8 in the Supporting Information). Namely, the complete resistance blockage is hard to achieve, but the ratio could be improved (e.g., the theoretical resistance on/off ratio for the 8-zigzag graphene nanoribbon shows more than $10^6\%$ with near zero off-resistance from the forbidden current transfer by imposing band structure symmetry, i.e., orbital symmetry as well as spin symmetry^[33,34]).

The relatively smaller ratio is attributed to the irregular electric field distribution in the transverse direction of the GNR (see simulated Figure S8 in the Supporting Information). Namely, the complete resistance blockage is hard to achieve. The ratio could be improved if the width of the GNR narrows and the diameter of FNW becomes small enough to impose band structure symmetry as a single crystal.^[33,34]

The GNR's I – V response is affected delicately by the state transitions in the FNW (Video S1, Supporting Information). As refs. ^[35,36] demonstrate, such response is determined by the charge carrier concentration in the graphene which in turn is controlled by the Fermi level and the doping. First, the electric field on the GNR consists of i) surface field that is created by the domain's surface charge $-\alpha \hat{S} \cdot \vec{P}(\vec{r}_s)$ which resides on the domain's outer surface and is simplified as a partially compensating charge to the depolarization field^[11,37] with a factor $0 < \alpha < 1$ and ii) gate field that is generated by the electrode. The surface field is determined by the polarization switching in the FNW, and the gate field is also affected indirectly by a switching of surface-charge screening (Figure S7, Supporting Information). Band diagrams (Figure 3) illustrate the influence of the electric field on the GNR under the FNW (see also Video S2 in the Supporting Information). The Fermi-level (FL) line connects the FL in each segment of the GNR approaching the continuum limit. The FL line is drawn in a simplified manner by connecting the FLs of its middle point γ and end points δ and η . Similarly, the Dirac-point (DP) line connects every DP located at zero for each segment of the GNR approaching the continuum limit. Positively shifted Dirac voltage suggests that the GNR is subject to a strong p-doping which is expected when graphene is exposed to moisture and oxygen in air on SiO₂ substrate^[38–41] (Figures S6 and S12, Supporting Information).

The doping-level (DL which is related to FL in the presence of chemical doping) line, which connects DLs for each segment of the GNR approaching the continuum limit, becomes a horizontal line below the DP line when doping is p-type; the DL line is the reference line from which the FL line is affected by the electric field. When the dipole field is radial, the surface charge is uniform (Figure 3: V2). The gate field is almost entirely screened (Figure S8: V2, Supporting Information). Thus, the FL line is flat except for points δ and η which are slightly lifted or lowered according to the polarity of V_G . In turn, the FL bends slightly by an amount related to the magnitude of V_G . However, when the dipole field is vertical, the surface charge density decays rapidly with increasing distance from point γ (Figure 3: V3). Thus, although the point γ of a FL line is still determined by the surface charge, points δ and η of a FL line are much affected by the unscreened gate field within the FNW's rim (Figure S8: V3, Supporting Information). Hence, there is a sharp decrease in the FL line from the center. The combination of two directions of gate field and four orientations of dipole field yields eight distinct distributions of electric field longitudinally along GNR; together with the chemical doping, such field distributions determine eight distinct FL lines of GNR. By contrast, the electron–hole symmetry in the conductivity gives a unimodal mapping from FL to conductivity, and thereby yields a hysteresis loop, that has up to eight vertices and has switching chirality, in GNR's I – V response. The loop has a butterfly shape with four vertices (v1–v4 in Figure 2b,c and Figure S9 (Supporting Information)) when involving two states,^[42] but a more complicated “fan-blade” shape with eight vertices (V1–V8 in Figure 2c) when involving four states. A detailed walkthrough of both the butterfly and “fan-blade” hysteresis loops is presented in Method S9 (see also Figures S7, S10–S15 and Videos S1 and S2 in the Supporting Information).

Qualitative features in the I – V hysteresis arise directly from two events. First, whenever the FL and DP lines cross, the

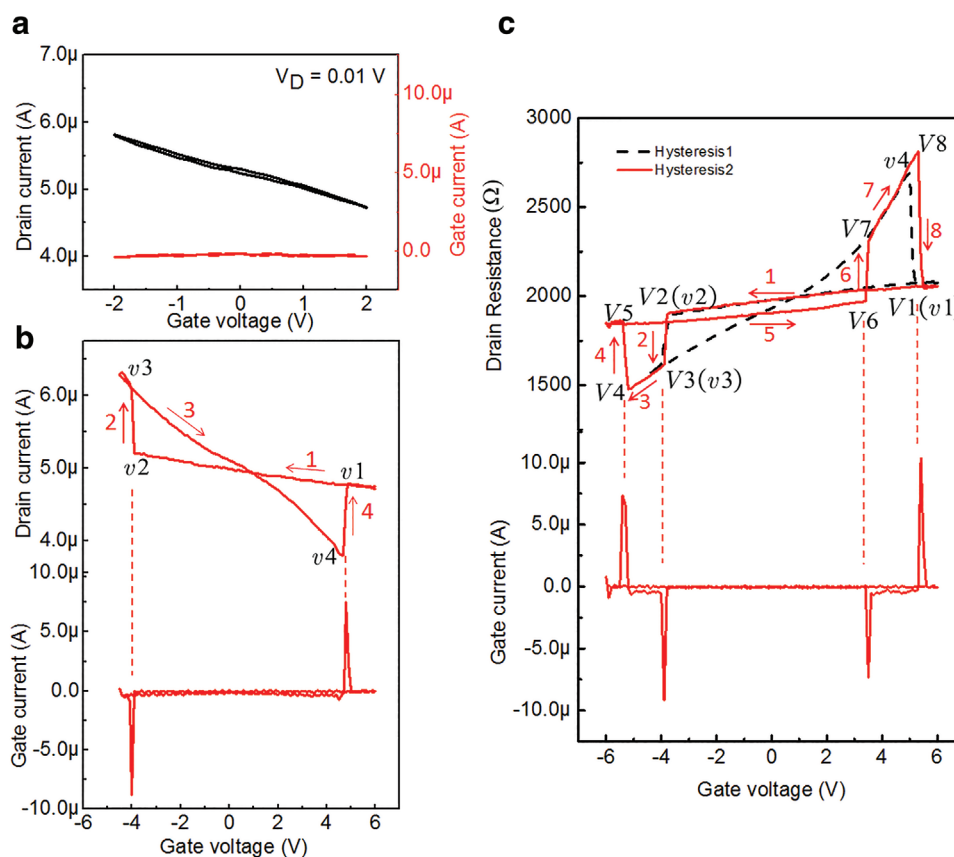


Figure 2. Characteristics of electronic device in top-gated architectures and electrical responses to the gate voltage sweep. a) No state transition exists for the low voltage sweep range between 2 and −2 V (type I). b) Drain current (upper) and gate current (lower) for the moderate gate voltage swept between +6 and −5 V (type II). Two state transitions occur, one in each of stages 2 and 4. c) Drain resistance (upper solid hysteresis 2 in red) and gate current (lower) for the large gate voltage swept between +6 and −6 V (type III). Four-state transitions occur, one in each of stages 2, 4, 6, and 8. Black dashed hysteresis 1 refers to type II sweep for reference. See also Video S2 (Supporting Information).

resistance increases quickly, as if a blockage occurs in the corresponding GNR segment to dominate the total resistance but not to completely block the circuit due to the intrinsic conductivity at a finite temperature.^[43,44] Second, the doping type determines the overall orientation of the hysteresis loop because it will determine whether the lifting/lowering of the FL will increase/decrease the conductivity.

Here, the domain wall effect in the FNW of diameter 250 nm (big enough to form numerous domain walls in our system, which will be discussed below) was not considered in our simplistic key model. One could analyze the quaternary polarization switching in terms of the Landau free energy based on the long-range elastic and electrostatic interactions, i.e., in view of domain elasticity and electric polarization including 90° polarization.^[26,27,29,45–51] However, our key aims in this work are: 1) the first experimental demonstration of the quaternary polarization switching which could be useful for quaternary-bit manipulation and 2) a simplistic qualitative model to explain such phenomena. We simplified the FNW with multidomains as homogeneous medium with a uniform dielectric constant. Even though the domain wall effect significantly affects the nonuniform distribution of dipole density in a radial polarization state of the FNW, its contribution to the free energy is

less significant than that of depolarization effect in a vertical polarization state (see Method S7 in the Supporting Information). Though the domain wall effect cannot be neglected, the system with a large number of domains due to a big enough NW diameter is roughly treated like a homogeneous dielectric medium, as a simple modeling study. However, for a system with a small number of domains, the domain's formation significantly affects the free energy of system due to inhomogeneity. In such a case, the domain wall effect should be carefully taken into account. We believe that our simple model in the present system is useful in explaining the experimental key phenomenon.

3. Conclusion

We have observed and explain new transitions among four states of the polarization in a semicircular top-gated FNW which forms a unique FNW–GNR–FET together with an underlying biased GNR. The state transitions are explained within LGT. The consequent exotic hysteresis of GNR's I – V response is explained graphically by the interplay of FL, DP, and DL lines. These new ferroelectric state transitions may stimulate a new

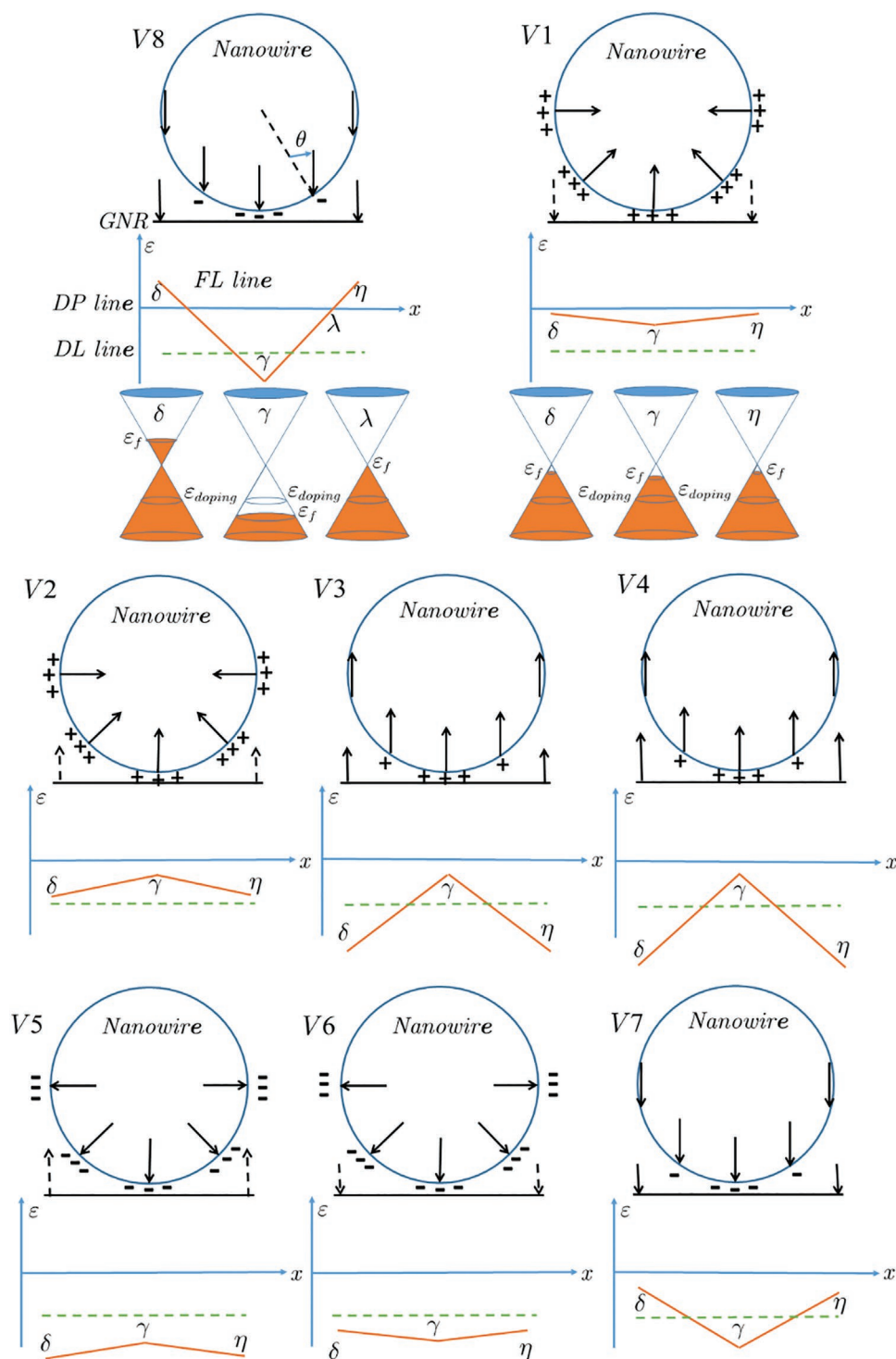


Figure 3. Band diagrams, including the Fermi level (FL), Dirac point (DP), and doping level (DL) lines, explain GNR resistance in various polarization states of the FNW. Solid arrow inside of FNW: dipole moment. Solid arrow on GNR: nonscreened gate field. Dashed arrow on GNR: almost-screened gate field. +/− symbol: the surface charge. The coordinate frame: the x-axis is the DP line, while the y-axis is the energy level. Green dashed line: the DL line below the DP line for p-doping. The FL line in orange is determined by distinct combinations of the gate field and polarization states of FNW. The enclosed area between FL and DP lines determines the conductivity on GNR, giving vortices of the GNR's I – V hysteresis shown in Figure 2: v1–v4 for moderate V_G sweep (type II), while v1–v8 for the large sweep (type III). In a vertical state (e.g., V8), the gate field below the rim of FNW's diameter is nonscreened. Dispersions show that the FLs at the two end points δ and η are in the conducting band, while that at the middle point γ is in valence band. FL and DP lines must cross at point λ . But in a radial state (e.g., V1(v1)), the surface charge is uniform, screening the gate field onto GNR. In result, the FL line is almost flat with the similar dispersions at the ends and in the middle of GNR. See also Video S2 (Supporting Information).

field of ferroelectric research. For instance, the four polarization states in FNW provide intrinsic quaternary digit in a non-volatile memory and the switching of the hysteresis chirality in a FNW–GNR–FET has potential in algebraic operation of quaternary-digit information.^[52] The easy all-NW-based and self-aligned fabrication approach used to make FET is an important step toward low-cost commercialization of highly sophisticated nanoelectronics. Given the boost in the storage capacity by the intrinsic quaternary-digit information storage with supra-binary ferroelectricity, our findings represent a major step forward in device miniaturization which includes a reduction of read-and-write heads as well as the physical size of the storage media.

Supporting Information

Supporting Information is available from the Wiley Online Library or from the author.

Acknowledgements

This research was supported by the National Honor Scientist Program (Grant No. 2010-0020414) and the Pioneer Research Center Program ICT and Future Planning (Grant No. 2012-0009460) through the National Research Foundation of Korea. This work was also supported by the National Research Foundation of Korea (NRF) grant funded by the Korea government (Ministry of Science and ICT) (Grant No. NRF-2016R1A3B1908431) and the Creative-Pioneering Researchers Program through Seoul National University (SNU).

Conflict of Interest

The authors declare no conflict of interest.

Author Contributions

W.X. and L.W. contributed equally to this work. W.X. designed and conducted most of the experiments. L.W. analyzed the polarization state transitions. D.C.Y. contributed to the electric field simulation. A.H. contributed to the free energy analysis. Y.L. contributed to the fabrication of fluorinated NW. C.P. commented the paper. T.-W.L. came up with the idea of creating the one-step self-aligned GNR FET. W.X., L.W., and K.S.K. wrote the paper. L.W., D.C.Y., and K.S.K. revised the paper. T.-W.L. and K.S.K. guided the project. K.S.K. acknowledged the reviewers' careful comments.

Data Availability Statement

The data that support the findings of this study are available from the corresponding author upon reasonable request.

Keywords

ferroelectric nanowires, field-effect transistors, graphene nanoribbons, Landau–Ginzburg theory, quaternary polarization switching

Received: March 12, 2021

Revised: April 26, 2021

Published online:

- [1] J. Wang, J. B. Neaton, H. Zheng, V. Nagarajan, S. B. Ogale, B. Liu, D. Viehland, V. Vaithyanathan, D. G. Schlom, U. V. Waghmare, N. A. Rabe, K. M. Spaldin, M. Wuttig, R. Ramesh, *Science* **2003**, 299, 1719.
- [2] S. Horiuchi, Y. Tokura, *Nat. Mater.* **2008**, 7, 357.
- [3] Q. M. Zhang, V. Bharti, X. Zhao, *Science* **1998**, 280, 2101.
- [4] M. Li, H. J. Wondergem, M.-J. Spijkman, K. Asadi, I. Katsouras, P. W. M. Blom, D. M. de Leeuw, *Nat. Mater.* **2013**, 12, 433.
- [5] *Physics of Ferroelectrics: A Modern Perspective*, Topics in Applied Physics, Vol. 105 (Eds: K. M. Rabe, C. H. Ahn, J.-M. Triscone), Springer, Berlin, Germany **2007**.
- [6] A. K. Tripathi, A. J. J. M. van Breemen, J. Shen, Q. Gao, M. G. Ivan, K. Reimann, E. R. Meinders, G. H. Gelinck, *Adv. Mater.* **2011**, 23, 4146.
- [7] J. I. Sohn, S. S. Choi, S. M. Morris, J. S. Bendall, H. J. Coles, W.-K. Hong, G. Jo, T. Lee, M. E. Welland, *Nano Lett.* **2010**, 10, 4316.
- [8] J. W. Jeong, Y.-E. Choi, W.-S. Kim, J.-H. Park, S. Kim, S. Shin, K. Lee, J. Chang, S.-J. Kim, K. R. Kim, *Nat. Electron.* **2019**, 2, 307.
- [9] A. S. Tayi, A. K. Shveyd, A. C.-H. Sue, J. M. Szarko, B. S. Rolczynski, D. Cao, T. J. Kennedy, A. A. Sarjeant, C. L. Stern, W. F. Paxton, W. Wu, S. K. Dey, A. C. Fahrenbach, J. R. Guest, H. Mohseni, L. X. Chen, K. L. Wang, J. F. Stoddart, S. I. Stupp, *Nature* **2012**, 488, 485.
- [10] J. F. Scott, A. Hershkovitz, Y. Ivry, H. Lu, A. Gruverman, J. M. Gregg, *Appl. Phys. Rev.* **2017**, 4, 041104.
- [11] R. Kretschmer, K. Binder, *Phys. Rev. B* **1979**, 20, 1065.
- [12] M. Hoffmann, F. P. G. Fengler, M. Herzig, T. Mittmann, B. Max, U. Schroeder, R. Negrea, P. Lucian, S. Slesazeck, T. Mikolajick, *Nature* **2019**, 565, 464.
- [13] H. Kawai, *Jpn. J. Appl. Phys.* **1969**, 8, 975.
- [14] J. G. Bergman, J. H. McFee, G. R. Crane, *Appl. Phys. Lett.* **1971**, 18, 203.
- [15] S. Bae, H. Kim, Y. Lee, X. Xu, J.-S. Park, Y. Zheng, J. Balakrishnan, T. Lei, H. R. Kim, Y. I. Song, Y.-J. Kim, K. S. Kim, B. Ozyilmaz, J.-H. Ahn, B. H. Hong, S. Iijima, *Nat. Nanotechnol.* **2010**, 5, 574.
- [16] K. S. Kim, Y. Zhao, H. Jang, S. Y. Lee, J. M. Kim, K. S. Kim, J.-H. Ahn, P. Kim, J.-Y. Choi, B. H. Hong, *Nature* **2009**, 457, 706.
- [17] S.-Y. Min, T.-S. Kim, B. J. Kim, H. Cho, Y.-Y. Noh, H. Yang, J. H. Cho, T.-W. Lee, *Nat. Commun.* **2013**, 4, 1773.
- [18] W. Xu, H.-K. Seo, S.-Y. Min, H. Cho, T.-S. Lim, C.-Y. Oh, Y. Lee, T.-W. Lee, *Adv. Mater.* **2014**, 26, 3459.
- [19] J. B. Lando, W. W. Doll, *J. Macromol. Sci., Part B: Phys.* **1968**, 2, 205.
- [20] W. A. Yee, M. Kotaki, Y. Liu, X. Lu, *Polymer* **2007**, 48, 512.
- [21] K. Tashiro, K. Takano, M. Kobayashi, Y. Chatani, H. Tadokoro, *Polymer* **1984**, 25, 195.
- [22] J. Miao, R. S. Bhatta, D. H. Reneker, M. Tsige, P. L. Taylor, *Polymer* **2015**, 56, 482.
- [23] P. Sharma, T. J. Reece, S. Ducharme, A. Gruverman, *Nano Lett.* **2011**, 11, 1970.
- [24] J. Miao, Private communication.
- [25] D. Zhao, T. Lenz, G. H. Gelinck, P. Groen, D. Damjanovic, D. M. de Leeuw, I. Katsouras, *Nat. Commun.* **2019**, 10, 2547.
- [26] J. Hong, G. Catalan, D. N. Fang, E. Artacho, J. F. Scott, *Phys. Rev. B* **2010**, 81, 172101.
- [27] J. Hong, D. Fang, *Appl. Phys. Lett.* **2008**, 92, 012906.
- [28] The radial electric field line cannot merge at the center of the nanowire without charge source.
- [29] R. Ahluwalia, N. Ng, A. Schilling, R. G. P. McQuaid, D. M. Evans, J. M. Gregg, D. J. Srolovitz, J. F. Scott, *Phys. Rev. Lett.* **2013**, 111, 165702.
- [30] P. Sharma, D. Wu, S. Poddar, T. J. Reece, S. Ducharme, A. Gruverman, *J. Appl. Phys.* **2011**, 110, 052101.
- [31] Y. Zheng, G.-X. Ni, C.-T. Toh, C.-Y. Tan, K. Yao, B. Özyilmaz, *Phys. Rev. Lett.* **2010**, 105, 166602.
- [32] D. Ielmini, S. Ambrogio, *Nanotechnology* **2020**, 31, 092001.

- [33] W. Y. Kim, K. S. Kim, *Nat. Nanotechnol.* **2008**, 3, 408.
- [34] W. Y. Kim, K. S. Kim, *Acc. Chem. Res.* **2010**, 43, 111.
- [35] A. I. Kurchak, E. A. Eliseev, S. V. Kalinin, M. V. Strikha, A. N. Morozovska, *Phys. Rev. Appl.* **2017**, 8, 024027.
- [36] A. I. Kurchak, A. N. Morozovska, E. A. Eliseev, S. V. Kalinin, M. V. Strikha, *Acta Mater.* **2018**, 155, 302.
- [37] X. Q. Chen, H. Yamada, T. Horiuchi, K. Matsushige, S. Watanabe, M. Kawai, P. S. Weiss, *J. Vac. Sci. Technol., B: Microelectron. Nanometer Struct.–Process., Meas., Phenom.* **1999**, 17, 1930.
- [38] T. O. Wehling, A. I. Lichtenstein, M. I. Katsnelson, *Appl. Phys. Lett.* **2008**, 93, 202110.
- [39] S. Ryu, L. Liu, S. Berciaud, Y.-J. Yu, H. Liu, P. Kim, G. W. Flynn, L. E. Brus, *Nano Lett.* **2010**, 10, 4944.
- [40] Y. Yang, R. Muralia, *Appl. Phys. Lett.* **2011**, 98, 093116.
- [41] M. R. Rezapour, C. W. Myung, J. Yun, A. Ghassami, N. Li, S. U. Yu, A. Hajibabaei, Y. Park, K. S. Kim, *ACS Appl. Mater. Interfaces* **2017**, 9, 24393.
- [42] B. Drincic, X. Tan, D. S. Bernstein, *Automatica* **2011**, 47, 2658.
- [43] A. H. Castro Neto, F. Guinea, N. M. R. Peres, K. S. Novoselov, A. K. Geim, *Rev. Mod. Phys.* **2009**, 81, 109.
- [44] W. Xu, L. Wang, Y. Liu, S. Thomas, H.-K. Seo, K.-I. Kim, K. S. Kim, T.-W. Lee, *Adv. Mater.* **2015**, 27, 1619.
- [45] N. Balke, S. Choudhury, S. Jesse, M. Huijben, Y. H. Chu, A. P. Baddorf, L. Q. Chen, R. Ramesh, S. V. Kalinin, *Nat. Nanotechnol.* **2009**, 4, 868.
- [46] R. Ahluwalia, M. B. Sullivan, D. J. Srolovitz, J. W. Zheng, A. C. H. Huan, *Phys. Rev. B* **2008**, 78, 054110.
- [47] A. N. Morozovska, M. D. Glinchuk, E. A. Eliseev, *Phys. Rev. B* **2007**, 76, 014102.
- [48] R. Ahluwalia, T. Lookman, A. Saxena, R. C. Albers, *Phys. Rev. Lett.* **2003**, 91, 055501.
- [49] R. Ahluwalia, T. Lookman, A. Saxena, *Acta Mater.* **2004**, 52, 209.
- [50] S. Chowdhury, Y. L. Li, C. E. Krill III, L. Q. Chen, *Acta Mater.* **2005**, 53, 5313.
- [51] L. Chen, J. Quyang, C. S. Ganpule, V. Nagarajan, R. Ramesh, A. L. Roytburd, *Appl. Phys. Lett.* **2004**, 84, 254.
- [52] T.-H. Kim, S. Cheon, H. W. Yeom, *Nat. Phys.* **2017**, 13, 444.